Efficient sorting of free electron orbital angular momentum

2017 New J. Phys. 19 023053

(http://iopscience.iop.org/1367-2630/19/2/023053)

New Journal of Physics
The open access journal at the forefront of physics

Deutsche Physikalische Gesellschaft DPG
IOP Institute of Physics

Published in partnership with: Deutsche Physikalische Gesellschaft and the Institute of Physics

OPEN ACCESS

RECEIVED
26 September 2016

REVISED
8 February 2017

ACCEPTED FOR PUBLICATION
9 February 2017

PUBLISHED
27 February 2017

PAPER

Efficient sorting of free electron orbital angular momentum

Benjamin J McMorran[1], **Tyler R Harvey**[1] **and Martin P J Lavery**[2]

[1] Department of Physics, University of Oregon, Eugene, OR, United States of America
[2] School of Engineering, University of Glasgow, Glasgow G12 8QQ, Scotland, United Kingdom

E-mail: mcmorran@uoregon.edu

Keywords: orbital angular momentum, electron vortex, electron microscopy

Abstract

We propose a method for sorting electrons by orbital angular momentum (OAM). Several methods now exist to prepare electron wavefunctions in OAM states, but no technique has been developed for efficient, parallel measurement of pure and mixed electron OAM states. The proposed technique draws inspiration from the recent demonstration of the sorting of OAM through modal transformation. We show that the same transformation can be performed on electrons with electrostatic optical elements. Specifically, we show that a charged needle and an array of electrodes perform the transformation and phase correction necessary to sort OAM states. This device may enable the analysis of the spatial mode distribution of inelastically scattered electrons.

1. Introduction

Electrons scattered by an interaction with matter, such as from individual atoms, molecules, or materials, acquire a spectrum of energies, linear momenta, and spin polarizations. Information about the event is encoded in these various degrees of freedom by the electron's wavefunction. Recently, several groups demonstrated control of the orbital angular momentum (OAM) of freedom of free electrons [1–3]. Myriad techniques for generating electron OAM states now exist, including material and magnetic spiral phase plates [1, 4–6], phase [7–9] and amplitude [2, 10] diffraction gratings, and mode conversion [11]. Exchange of OAM between a target specimen and a fast electron could provide information about the structural chirality [12, 13] and out-of-plane magnetization of the target [14–16]. In these applications, the electrons can scatter to many different final OAM states, and measurement of the final OAM distribution can provide new information about the scattering targets. However, there are currently no measurement techniques that can efficiently and quantitatively measure the OAM distribution of free electrons.

In 2010, Berkhout *et al* [17] demonstrated a new method to efficiently sort OAM states of light using four refractive optical elements. The apparatus transforms an azimuthal phase at the input into a linear phase at the output, such that OAM components at the input are mapped into separate linear momentum states at the output. This ability to measure superpositions and mixed states of optical OAM enables parallel OAM measurement. The apparatus has been rapidly employed for a range of optical applications in both fundamental research [18, 19], quantum information [20], and communications [21, 22]. As shown in figure 1(a), the apparatus is based on two custom-made non-spherical refractive optical components, the phase unwrapper U and the phase corrector C, with two lenses L1 and L2 used to the Fourier transform the output of each.

The first optical element (U and L1 in figure 1) is a log-polar transformer [23] that transforms a set of concentric rings at the input plane into a set of parallel lines at the back focal plane of the lens—or, equivalently, OAM states into planar waves. The phase profile of this unwrapper element is described by equation (1) in [17]:

$$\varphi_{\mathrm{U}}(x, y) = \frac{1}{\Delta t}\left[y \arctan\left(\frac{y}{x}\right) - x \ln\left(\frac{\sqrt{x^2 + y^2}}{b}\right) + x \right], \tag{1}$$

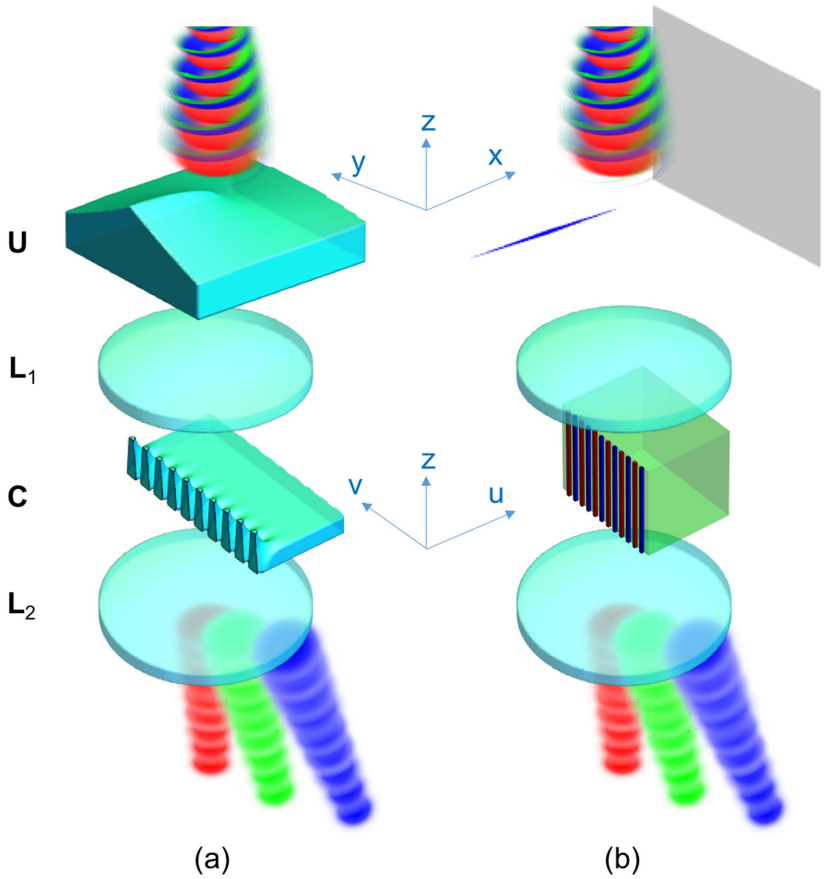

Figure 1. Schematic of the optical arrangement of OAM-sorting devices for (a) light and (b) electrons. Different OAM states are shown in different colors. Mixed OAM states are incident on the top of both systems, each of which consists of four elements. A phase unwrapper element U in the front focal plane of a lens L1 is followed by a phase corrector element C in the back focal place of L1. For electrons, the proposed element U is a charged needle or knife edge, and the corrector element C is an array of electrodes with alternating bias. Immediately after the corrector element C, different OAM components are separated in momentum space. At the bottom of each device, a Fourier-transforming lens L2 separates OAM components into different spots in real space at the output.

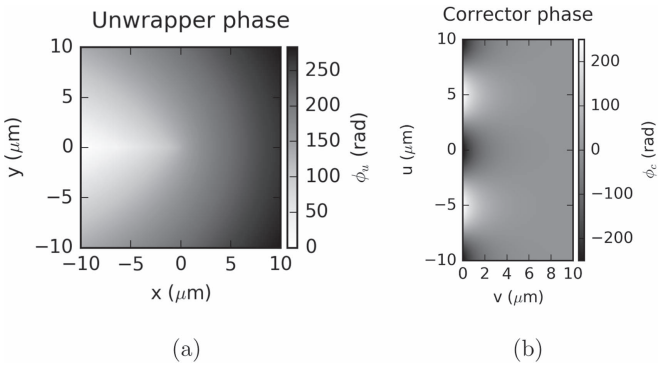

Figure 2. Phase profiles of the (a) unwrapper element U described in equations (1) and (b) the corrector element C described in equation (4). In (a), the lowest phase (white) occurs at the position of the needle. Both plots use parameters expressed in table 1.

where Δt is a lengthscale that sets the separation distance between OAM states in the output plane, and b is a lengthscale that determines the position of the unwrapped beam in the corrector plane. A plot of the phase distribution for this lens is shown in figure 2(a).

2. Electrostatic OAM unwrapper for electrons

To imprint the phase profile described in equation (1) onto an electron wavefunction, one could use either refractive or diffractive wavefront-shaping techniques. In light optics, there are established methods for

fabricating custom phase plates out of transparent material such as glass. However, while thin film phase plates for electrons are possible [6], they contaminate easily and are difficult to fabricate. Finally, no material is sufficiently electron-transparent to imprint the large phases required for sorting OAM. Arbitrary electron phase profiles can be imprinted holographically using nanofabricated diffractive optics [7, 8]. However, the smaller but still significant inelastic scattering in the material, the small diffraction angles, low diffraction efficiency, and finite size of the diffractive structures make the use of such holograms for an OAM mode sorter impractical.

Instead, a relatively simple electrostatic phase plate consisting of a charged needle and a conductive plate can be used to imprint a phase equivalent to equation (1) onto a charged particle wave. The phase that the tip of a charged needle imparts to an electron has been studied previously by several different groups [24–26]. Matteucci *et al* [24] calculated this analytically by first considering the electrostatic potential $V(\mathbf{r})$ around an infinitesimally thin wire of finite length and uniform charge density placed a distance h away from a flat conducting plate. The spatially varying phase shift a potential $V(\mathbf{r})$ imparts to an electron plane wave of energy E and relativistically corrected wavelength λ traveling in the $+z$ direction can be calculated by the integral

$$\varphi(\mathbf{r}) = C_E \int_{-\infty}^{\infty} V(\mathbf{r})\,\mathrm{d}z, \tag{2}$$

where C_E is a constant that depends only on the energy of the beam [27] ($C_E = 6.53$ mrad V^{-1} nm^{-1} for 300 keV electrons).

In appendix A, we adapt Matteucci *et al*'s result (equation (4) in [24]) for the purpose of imprinting equation (1). We show that if the electron beam is localized around the needle tip nearest the plate electrode, and the length of the needle and its separation from the plate are sufficiently large, this arrangement imprints the appropriate unwrapping phase for sorting electron OAM:

$$\varphi_{\mathrm{U}}(x, y) = \frac{QC_E}{4\pi\epsilon_0 L}\left[y \arctan\left(\frac{y}{x}\right) - x \ln\left(\frac{\sqrt{x^2+y^2}}{L}\right)\right] + \varphi_0, \tag{3}$$

where L is the length of the needle, E is the kinetic energy of the electron beam, and φ_0 is a uniform phase common to all paths, which is unobservable at the detector. With the exception of a missing linear phase, we see that equation (3) exactly matches equation (1) if $b = L$ and $\frac{Q}{L} = \frac{4\pi\epsilon_0}{C_E \Delta t}$. This discrepancy is unimportant, as a linear phase in the unwrapper plane corresponds to a position offset in the corrector plane that can be easily provided by position alignment optics (based on static in-plane magnetic or electric fields) found in the transmission electron microscope.

There are several possible methods for practical realization of such an electrostatic element in an electron microscope, as discussed further in appendix B. A thin insulating wire could provide the constant line charge density assumed for the derivation of equation (1), although in an actual device the charge density could be affected by the incident beam current and could fluctuate in time. On the other hand, a conducting wire fabricated such that its physical surface coincides with the equipotential surface of a constant line charge may be more easily tunable and more robust against changes in the incident beam current. In appendix B, we use simulations to demonstrate that such needles can impart the appropriate unwrapper phase modulation with excellent fidelity, and we find that this is insensitive to electrostatic boundary conditions. The inner conductive surfaces of an electron microscope are typically grounded and are hundreds of microns to millimeters away from the electron beam, and in such limits these surfaces will have little effect on the phase imparted by the needle.

When using the proposed device to measure OAM distributions of electrons scattered from a specimen in a TEM, it is important to realize that these orbital states will originate from different locations in the sample. For example, electron orbital states could be generated by scattering from each atom in a material, and so the electron vortices will have different centers each offset from one another. This results in a complicated distribution in the near field of the specimen. To ensure all of these offset orbital states are aligned with the input of the proposed OAM sorter, the input of the sorter should be positioned in the far-field of the specimen where the orbital mode distribution will be spatially coherent and all electron vortices will be concentric. For actual experiments, the needle-based phase unwrapper should therefore be placed in the back focal plane of the sample. A modified aperture holder provides a convenient way to install, position, and electrically bias the needle-based corrector. Such holders have already been developed for a variety of TEMs in order to control charged Möllendstedt biprism wires for use in electron holography.

We also note that an extended knife edge electrode could potentially be used instead of a charged needle. The 2D electrostatic potential of a semi-infinite plane of charge with it's edge along the z-axis has the same functional form as the desired unwrapper phase $\varphi_{\mathrm{U}}(x, y)$ (see Chapter 7 in [28]). Thus, an appropriately shaped knife-edge electrode aligned along the optical axis could provide an alternative design to the needle, if the length were long enough such that phase introduced near the beginning and end of the electrode were negligible. Such a design, however, might undesirably affect the amplitude of the incident electron wave.

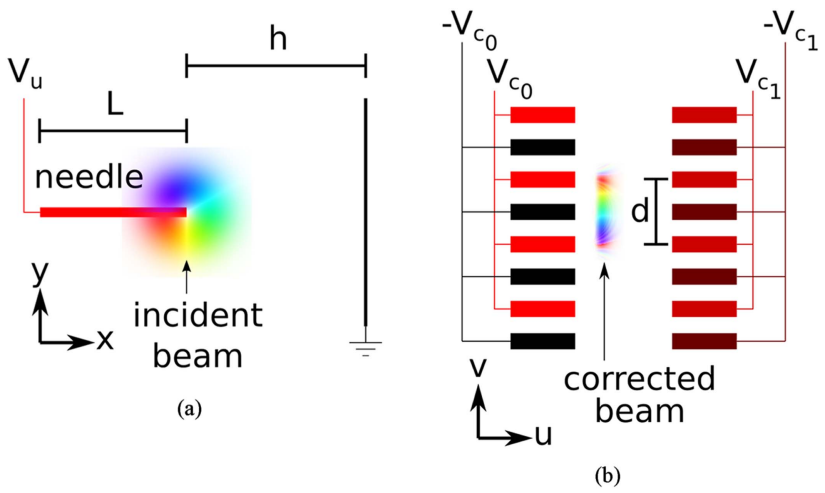

Figure 3. (a) Top-view cartoon of charged needle and ground plate used to produce the unwrapper phase. Electrons passing into the device near the right end of the needle will acquire the phase described by equation (3). (b) Top-view cartoon of example electrodes that could be used to produce the corrector phase, (4). Alternating very high (V_{C_0}) and very low ($-V_{C_0}$) voltages at the boundary at $u = 0$ produce a sinusoidal potential in the v-direction. Alternating weakly high (V_{C_1}) and weakly low ($-V_{C_1}$) voltages at the boundary at $u = u_1$ produce an exponential decay in the u-direction. The electrodes at $u = u_1$ are not physically necessary, as we show in figure C2b.

3. Electrostatic phase corrector for electrons

The phase unwrapper element is followed by a conventional electron lens system (L1). Simulations of the electron wave function in the back focal plane of this intermediate lens show that there are large variations in the phase due to the unwrapping operation. These phase variations must be removed by a second optical element to reveal the subtler OAM-dependent differences. This phase corrector (labeled 'C' in figure 1) is described by the following phase profile:

$$\varphi_C(u, v) = \frac{b}{\Delta t}\exp\left(-\frac{2\pi u}{d}\right)\cos\left(-\frac{2\pi v}{d}\right), \tag{4}$$

where, following the notation of Berkhout *et al* [17], we use (u, v) to describe the transverse coordinates of the transformed field in the corrector plane from the transverse coordinates of the input field. This corrector phase, shown in figure 2(b), is identical to the phase derived by Berkhout *et al* [17], using some re-labeled variables. To accurately correct the phase in this plane, the amplitude of this phase modulation must be proportional to $\frac{b}{\Delta t}$, and the lengthscale $d = \frac{\lambda f}{\Delta t}$, where f is the focal length of lens L1 between the unwrapper and corrector planes.

Electrostatic elements can also be employed to imprint this corrector phase. As the phase distribution is a solution to Laplace's equation in 2D, i.e. $\nabla^2\varphi_C(u, v) = 0$, we see that an electrostatic potential in 2D can take this form. We can approximate the 2D potential solution in 3D with a potential that varies slowly in z. Specifically, we can apply $\varphi_C(u, v)$ to an electron with a set of alternating electrodes, as shown in figure 3(b). As long as the longitudinal height D of the electrodes is much longer than the period d (see appendix C), and the thin grating condition, $\lambda D \ll d^2$ is satisfied, the variation of the potential in the longitudinal direction is negligible over the depth. The corrector phase can be written as

$$\varphi_C(u, v) = C_E D V_{C_0}\exp\left(\frac{-2\pi u}{d}\right)\cos\left(\frac{-2\pi v}{d}\right). \tag{5}$$

We see that we get the appropriate φ_C (equation (4)) if $C_E D V_{C_0} = \frac{bd}{\lambda f}$ and $V_{C_1} = V_{C_0}\exp\left(-\frac{2\pi u_1}{d}\right)$. Further analysis (see appendix C) shows that it could be practical to remove the reference electrodes at $u = u_1$ if the nearest grounded surface is sufficiently far away (at some distance much larger than d).

As shown in figures 4(b), and (e), immediately after the corrector the phase of the electron beam is flattened, such that an input state with OAM quantum number m is transformed here into a bar-shaped distribution with a phase that linearly varies in the v-direction from 0 to $2\pi m$ over the width of the beam profile. The slope of this corrected phase ramp is inversely proportional to the width of the beam profile in the v-direction, equal to Δt. Thus, after the Fourier-transforming lens L2, the initial orbital modes are focused at the output plane into separate lines (figure 4) with a final spacing of

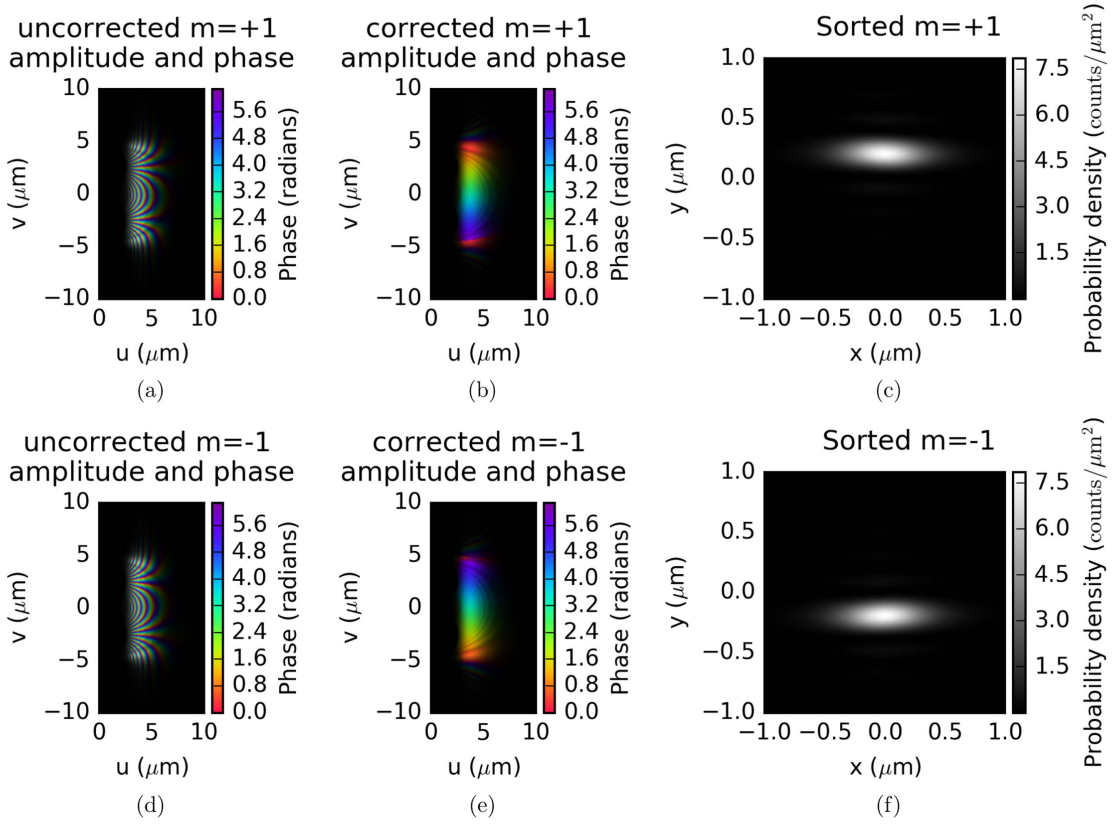

Figure 4. Illustration of the action of the device. The unwrapper U and intermediate lens L1 produces a beam in the corrector plane that has width d in the v-direction and that has rapid phase variations (a) and (d). The corrector C removes the rapid phase variations to produce plane wave-like beams in the corrector planes (b)and (e) which correspond to deflected spots in the output planes (c) and (f). These simulations assume ideal unwrapper and corrector phases (equations (3) and (5)) with parameters shown in table 1.

$$\Delta t = \frac{\lambda f}{d}. \tag{6}$$

4. Design parameters and simulated outputs

Lavery *et al* separated OAM states of light with a wavelength of $\lambda = 632.8$ nm, lens focal length $f = 300$ mm, a corrector period $d = 8$ mm and therefore an unmagnified separation of $\Delta t = 23.73$ μm [18]. As preparation of a collimated photon OAM state with a waist on the order of 10 μm is straightforward, this separation is sufficient.

The orders of magnitude of these parameters are wildly different for electrons, but good separation is similarly straightforward. One set of possible parameter values to achieve this is listed in table 1. With a needle length of $L \sim 50$ μm, an incident beam waist on the order of 1 μm is physically reasonable. Separation on the order of $\Delta t = 0.2$ μm can be achieved in a transmission electron microscope at 300 kV with $\lambda \sim 1.97$ pm and a corrector period of $d \sim 10$ μm if the focal length of the lens between the needle and corrector, L1, is $f \sim 100$ cm. Several lenses with focal lengths in the 1 cm to 10 cm range can be combined to more practically produce a 1 meter focal length over a much shorter distance.

To review, the parameters of this arrangement are: (a) the charge Q added to the needle-based unwrapper phase plate, (b) the length of the needle L, (c) the voltage V_{C_0} applied to the corrector electrodes, (d) the spatial periodicity d of the corrector electrodes, and (e) the focal length of the lenses f. We have offered one possible combination of parameters here, but this may of course be tuned according to the application.

Figures 4–6 show the action of a sorter with these parameters on various input states. Note that, just as with an optical OAM sorter, the electron device sorts multiple input OAM states identically regardless of whether they are in coherent superpositions (figures 5(c) and (g)) or incoherent mixtures (figures 5(d) and (h)). As shown in the simulation in figure 6, the electron OAM sorter could also be used for orbital mode decomposition of arbitrary wavefunctions, which could be used to reveal hidden chiral asymmetries in electron-scattering targets.

Table 1.

Sorter parameter	Magnitude
λ	1.97 pm
f	1 m
d	10 μm
$b = L$	50 μm
$V_{C_0} D$	39 V μm
Q/L	8.5 p C m^{-1}
V_U	0.63 V

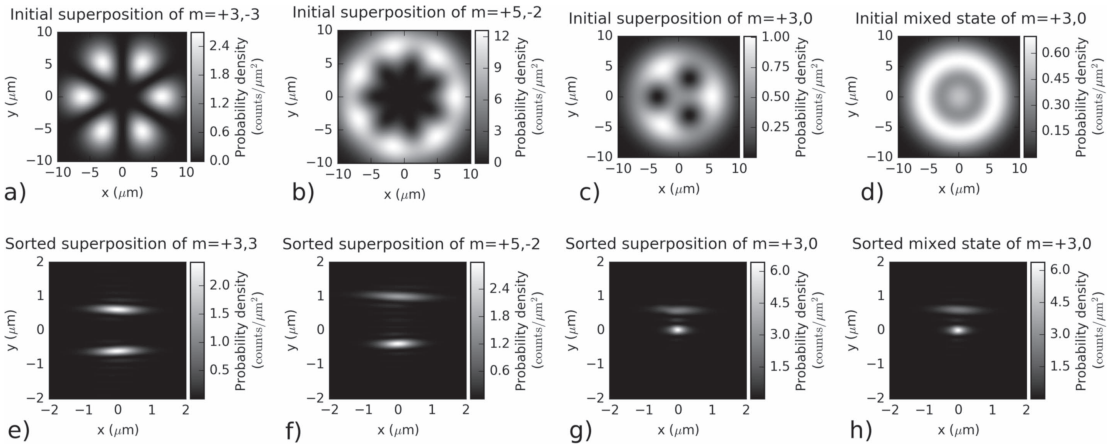

Figure 5. The simulated (a)–(d) input and (e)–(h) output of the proposed electron OAM sorter using parameters shown in table 1. Note that the outputs (e)-(h) are zoomed-in for clarity.Input states are Laguerre–Gaussian modes with a 5 μm beam waist and (a) superposed $m = +3$ and $m = -3$, (b) superposed $m = +5$ and $m = -2$, (c) superposed $m = 3$ and $m = 0$, and (d) mixed $m = +3$ and $m = 0$. Each electron OAM component at the input gets mapped onto a separate region in space at the output, which is viewed directly using TEM imaging optics. In this way, a spectrum of electron OAM states can be efficiently recorded in parallel.

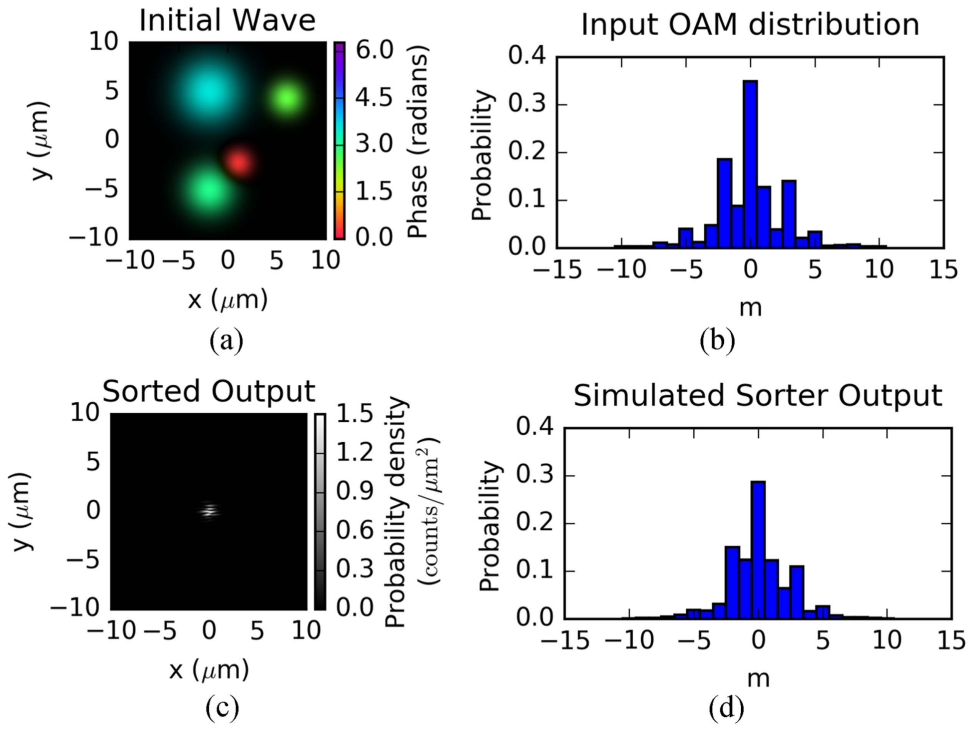

Figure 6. (a) Initial random wavefunction with non-trivial orbital angular momentum distribution; amplitude is shown as brightness and phase is shown as hue; (b) calculated orbital angular angular momentum distribution; (c) probability density of the random wavefunction passed through the sorter; (d) orbital angular momentum distribution calculated by binning the output of the sorter.

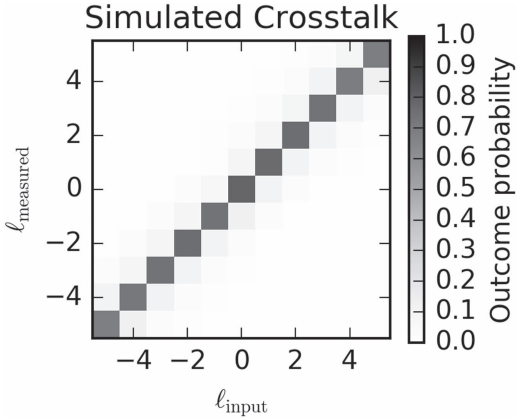

Figure 7. Crosstalk of the electron orbital angular momentum measurement with parameters shown in table 1. A perfect sorter would have outcome probabilities of exactly 1 for every $\ell_{\text{measured}} = \ell_{\text{input}}$ and 0 elsewhere. As with an optical OAM mode sorter, the crosstalk of this device is due to diffraction limit.

5. Crosstalk

An important figure of merit for a measurement device is the crosstalk: the rate of erroneous counts that occur when adjacent measurement outcomes are counted as the outcome of interest. In the proposed electron OAM sorter, there will be some crosstalk that arises from the diffraction limit. Input electron orbital modes separated by a single OAM quanta ($\Delta m = 1$) become plane waves just after the corrector element that are just slightly tilted from one another, with phase ramps that only differ by 2π across the width of the states. Thus, when focused onto an imaging detector by lens L2, these two states are only just resolvable. Figure 7 shows the crosstalk of an ideal electron OAM sorter, simulated with phases shown in equations (3) and (5) and parameters shown in table 1. In a real device, aberrations and misalignment of the electron beam are likely to further increase this minimum amount of crosstalk.

6. Conclusion

Knowledge of interactions in which a free electron exchanges OAM with a specimen can lead to insights into the properties of the object. However, many attempts by several groups to observe OAM transfer between a prepared focused electron with OAM and an atom have so far been unsuccessful, due to the fact that electrons are scattered into a superposition of orbital states. Here we described an electron-optical analog of the OAM sorter developed for photons. This device can non-destructively disperse the spectrum of electron OAM, providing a way to measure the OAM distribution of electrons scattered or ejected from atoms, molecules, and larger collections of matter. Thus, this could provide a completely new form of spectroscopy that can be used to probe the asymmetric structure of matter, atomic and molecular polarizations, and chiral interactions.

Acknowledgments

BJM and TRH were partially supported by the US Department of Energy, Office of Science, Basic Energy Sciences, under Award #DE-SC0010466, and partially supported by the National Science Foundation under Grant No. 1607733. MPJL is supported by the Royal Academy of Engineering Research Fellowship RF/131 and ESPRC First Grant EP/N032853/1. We thank Martin Linck of Corrected Electron Optical Systems GmbH for order-of-magnitude estimates of lens focal lengths that were helpful in assessing practical relevance. We thank Giulio Pozzi for helpful discussions about the needle.

Appendix A. Calculation of phase past charged needle

Here we consider electrons propagating in the z direction past an infinitesimally thin needle of constant charge density $\sigma = Q/L$, where L is the length of the needle. We consider that the needle lies on the x-axis with one tip at the origin and the other located at $x = -L$. The charged needle is oriented perpendicularly to a conducting plate that lies parallel to the y–z plane at $x = h$. The electrostatic potential of this arrangement can be written as

$$V(\mathbf{r}) = \frac{Q}{4\pi\epsilon_0 L}\ln\left[\left(\frac{x+L+\sqrt{(x+L)^2+y^2+z^2}}{x+\sqrt{x^2+y^2+z^2}}\right)\times\left(\frac{x-2h-L+\sqrt{(x-2h-L)^2+y^2+z^2}}{x-2h+\sqrt{(x-2h)^2+y^2+z^2}}\right)\right]. \tag{A.1}$$

Following [24], we use equation (2) to calculate the phase an electron plane wave acquires as it propagates through this potential:

$$\begin{aligned}\varphi_U(\mathbf{r}) = -\frac{QC_E}{4\pi\epsilon_0 L}\Bigg[&|y|\sin^{-1}\left(\frac{-x-L}{\sqrt{(x+L)^2+y^2}}\right) - |y|\sin^{-1}\left(\frac{-x}{\sqrt{x^2+y^2}}\right)\\ &+|y|\sin^{-1}\left(\frac{-x+2h+L}{\sqrt{(x-2h-L)^2+y^2}}\right) - |y|\sin^{-1}\left(\frac{-x+2h}{\sqrt{y^2+(x-2h)^2}}\right)\\ &- x\ln\left(\frac{\sqrt{(x+L)^2+y^2}}{\sqrt{x^2+y^2}}\right) - x\ln\left(\frac{\sqrt{(x-2h-L)^2+y^2}}{\sqrt{(x-2h)^2+y^2}}\right)\\ &- L\ln\left(\frac{\sqrt{(x+L)^2+y^2}}{\sqrt{(x-2h-L)^2+y^2}}\right) + 2h\ln\left(\frac{\sqrt{(x-2h-L)^2+y^2}}{\sqrt{(x-2h)^2+y^2}}\right)\Bigg].\end{aligned} \tag{A.2}$$

We consider a situation in which the incident electron beam is confined only to the region immediately adjacent to the tip of the needle nearest to the plate. If we take the distance h between the needle and the plate to be much larger than the region of interest, i.e. $h \gg \sqrt{x^2+y^2}$, we see some simplification. The third and fourth terms cancel, the sixth term goes to zero, and the last two terms go to a constant phase shift that depends only on L and h. Depending on the relative magnitudes of h and L, it is also possible to extract a linear phase in x from the latter three terms

$$\begin{aligned}\varphi_U(\mathbf{r}) = -\frac{QC_E}{4\pi\epsilon_0 L}\Bigg[&|y|\sin^{-1}\left(\frac{-x-L}{\sqrt{(x+L)^2+y^2}}\right) - |y|\sin^{-1}\left(\frac{-x}{\sqrt{x^2+y^2}}\right)\\ &- x\ln\left(\frac{\sqrt{(x+L)^2+y^2}}{\sqrt{x^2+y^2}}\right)\Bigg] + \varphi_0,\end{aligned} \tag{A.3}$$

where φ_0 is a constant 'background' phase that does not affect the sorter mechanism.

If we rewrite the inverse trigonometric functions, we see that the extra $|y|\frac{\pi}{2}$ terms cancel and we have

$$\begin{aligned}\varphi_U(\mathbf{r}) = -\frac{QC_E}{4\pi\epsilon_0 L}\Bigg[&|y|\cos^{-1}\left(\frac{x+L}{\sqrt{(x+L)^2+y^2}}\right) - |y|\cos^{-1}\left(\frac{x}{\sqrt{x^2+y^2}}\right)\\ &- x\ln\left(\frac{\sqrt{(x+L)^2+y^2}}{\sqrt{x^2+y^2}}\right)\Bigg] + \varphi_0.\end{aligned} \tag{A.4}$$

If we now take the length of the needle as large compared to the region of interest, i.e. $L \gg \sqrt{x^2+y^2}$, we see further simplification of the result. As $\cos^{-1}(1) = 0$, we are left with two terms With this approximation, the phase distribution induced onto an electron wave passing close to the tip of the needle is:

$$\varphi_U(\mathbf{r}) = -\frac{QC_E}{4\pi\epsilon_0 L}\left[-|y|\cos^{-1}\left(\frac{x}{\sqrt{x^2+y^2}}\right) + x\ln\left(\frac{\sqrt{x^2+y^2}}{L}\right)\right] + \varphi_0, \tag{A.5}$$

which we can finally rewrite, using the fact that $\cos^{-1}\frac{x}{\sqrt{x^2+y^2}} = \tan^{-1}\frac{|y|}{x}$, as

$$\varphi_U(\mathbf{r}) = \frac{QC_E}{4\pi\epsilon_0 L}\left[y\tan^{-1}\left(\frac{y}{x}\right) - x\ln\left(\frac{\sqrt{x^2+y^2}}{L}\right)\right] + \varphi_0. \tag{A.6}$$

Equation (A.6) is exactly the desired phase of the unwrapper element (equation (1)) minus a linear phase. The missing linear phase corresponds to a position shift in the output plane that can be easily corrected with readily available magnetostatic or electrostatic position alignment optics.

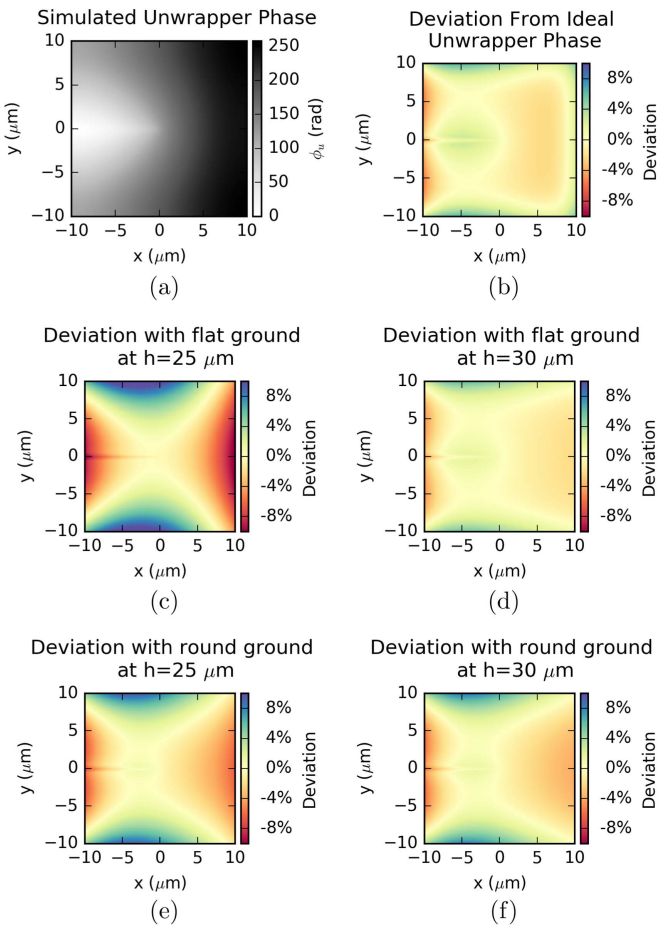

Figure B1. Simulations of the electron phase effects of a shaped conducting needle with physical surfaces defined to match equipotentials of a constant line charge density, with various boundary conditions. The electrostatic potential was calculated around a needle of length $L = 50\ \mu$m with various boundary conditions, and the phase imparted to the electron was calculated after traversing the region from $x = -10\ \mu$m to $x = +10\ \mu$m, $y = -10\ \mu$m to $y = +10\ \mu$m, and $z = -40\ \mu$m to $z = +40\ \mu$m. The von Neumann boundary condition $\nabla V \cdot \hat{\mathbf{n}} = 0$ was used for all boundaries. (a) Phase distribution imprinted by the needle on an electron wave passing through the simulated region. (b) Deviation of the phase shown in (a) from an ideal unwrapper phase described by equation (1). Deviation is defined as the difference between the simulated phase and the ideal phase, divided by the difference between the maximum and minimum ideal phase in the 20 μm × 20 μm region shown. (c) Deviation of a phase calculated from a simulation box with a flat ground plate (Dirichlet boundary) at $x = +25\ \mu$m. (d) Deviation of a phase calculated from a simulation box with a flat ground plate at $x = +30\ \mu$m. (e) Deviation of a phase calculated from a simulation box with a semi-cylindrical ground plate at a radius of $+25\ \mu$m from the end of the needle. (e) Deviation of a phase calculated from a simulation box with a semi-cylindrical ground plate at a radius of $+30\ \mu$m from the end of the needle.

Appendix B. Fidelity of the phase of proposed unwrapper element

It is well established that a thin, biased conducting needle does not maintain a constant line charge density [29, 30]. Experiments have shown that a thin, insulating needle aquires a negative charge under the incident electron beam [31], and it is possible that the charge density on such an insulating needle is nearly constant. However, it seems that the value of the charge density, and therefore the parameters of the sorter, might depend more strongly on the incident beam current than is desirable for a robust, tunable device.

A more controllable approach involves the use of a biased conductor with a physical surface fabricated to match the equipotential surfaces of a constant line charge density [29]. In particular, to produce a potential that corresponds to a line charge density Q/L and a length of the line charge L, the needle should be held at a voltage V_U with a surface defined by the equipotential

$$V_U = \frac{Q}{4\pi\epsilon_0 L} \ln\left(\frac{x + L + \sqrt{(x+L)^2 + y^2 + z^2}}{x + \sqrt{x^2 + y^2 + z^2}}\right) \tag{B.1}$$

which corresponds to equation (A.1) in the limit that $h \to \infty$.

We simulated the potential produced by the nearly hyperboloid tip described above, with a conducting surface at the equipotential $V_U = 8\frac{Q}{4\pi\epsilon_0 L}$. As equation (A.1) is a solution to Laplace's equation, i.e.

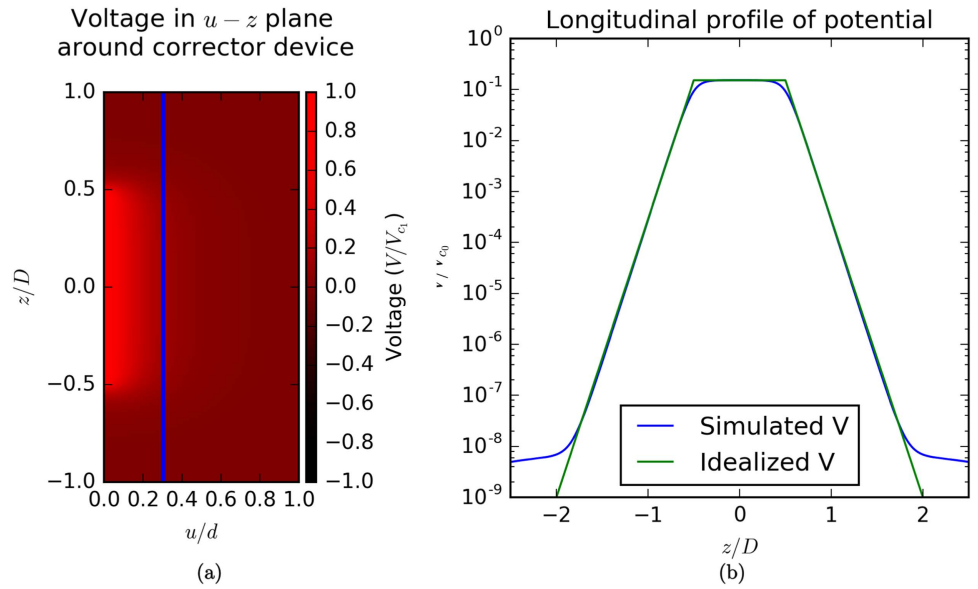

Figure C1. (a) Cross-section of simulated potential in the u–z plane at $v = 0$ showing rapid decay of potential outside the device. (b) Line plot of a simulated potential at $u = 0.3d$ in the u–z plane showing exponential decay of the potential outside the device. (blue) Simulated potential $V(u = 0.3d,\ v = 0,\ z)$, also shown as blue line in (a); (green) model of the potential that is constant inside the device and exponentially decays as $V \propto \exp\left(\pm\frac{2\pi(z \pm D/2)}{d}\right)$ outside the device. This simulation used a period d =1.0, a depth $D = 2.0$ (resulting in boundaries at $z = \pm 1.0$), arbitary V_{C_0}, and boundaries at $u = 0$, $u = 1.0$, $v = 0$, $v = 1.0$, $z = -50.0$ and $z = 50.0$ with a voxel size of 0.01 by 2^{-5} by 0.01.

$\nabla^2 V(x,\ y,\ z) = 0$, everywhere except at the position of the needle, we numerically solved Laplace's equation with a Dirichlet boundary given by equation (B.1). We tried several boundary conditions for the external boundaries to test the robustness of the potential against variations in the shape and location of the grounded conductor. The results of these simulations are shown in figure B1. The phases calculated with equation (2) from simulated potentials show excellent agreement with the ideal unwrapper phase, equation (A.6), regardless of boundary conditions, and especially as the distance h to the conducting plate is increased. When h is smaller (e.g. figure B1(c)), a noticeable astigmatic $y^2 - x^2$ phase is noticeable. This deviation is correctable using standard quadrupolar stigmators.

Appendix C. Fidelity of the phase of proposed corrector element

As the corrector phase solves Laplace's equation, it is straightforward to generate this phase with an electrostatic potential $V(u,\ v)$, following equation (2). We can approximate the two-dimensional solution to Laplace's equation $V(u,\ v)$ with a nearly z-independent three-dimensional solution. The simplest boundary conditions are constant over a range in z that we will call the depth, D. In particular, we can specify the $V(u,\ v)$ we want with boundaries at $u = 0$ and $u = u_1$. In other words

$$V(u_i,\ v,\ z) = \begin{cases} V(u_i,\ v) & |z| \leqslant \frac{D}{2}, \\ \text{free} & \text{elsewhere.} \end{cases} \tag{C.1}$$

We investigated these boundaries with a numerical solution to Laplace's equation. For figures C1 and C2(a), we set Dirichlet boundary conditions at two positions in u. In the range $|z| < \frac{D}{2}$, we set the Dirichlet boundary conditions

$$V(u = 0,\ v) = V_{C_0}\cos\left(-\frac{2\pi v}{d}\right), \tag{C.2}$$

$$V(u = u_0,\ v) = V_{C_1}\cos\left(-\frac{2\pi v}{d}\right), \tag{C.3}$$

where V_{C_0} and V_{C_1} are the peak potentials at $u = u_0 = 0$ and $u = u_1$, respectively, and d is the period in v. We see that, to satisfy Laplace's equation, we must have $V_{C_1} = V_{C_0}\exp\left(-\frac{2\pi u_1}{d}\right)$. We used periodic boundary conditions in v, and the von Neumann boundary condition $\boldsymbol{\nabla} V \cdot \hat{\mathbf{n}} = 0$ for all other boundaries. For figure C2(b), we used

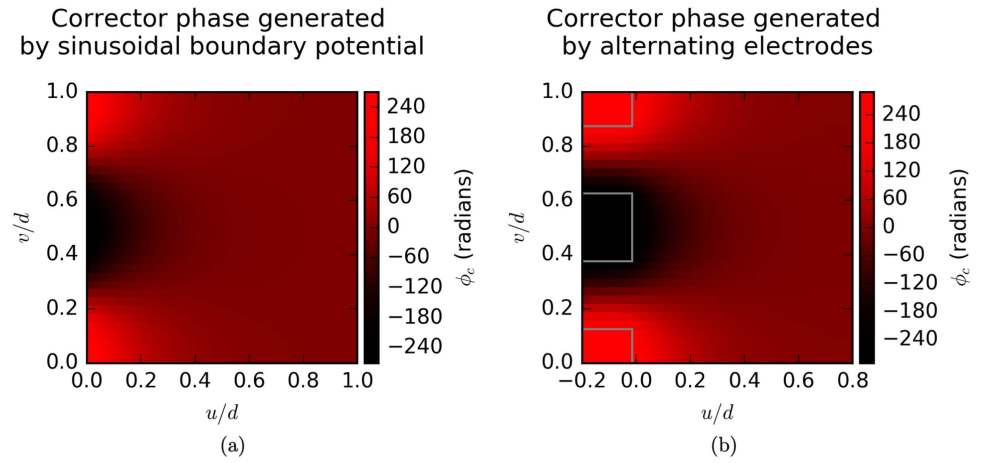

Figure C2. Corrector phase calculated by simulating the potential with two different sets of boundary conditions. (a) Phase calculated with potential set by a sinusoidally varying potential along $u = 0$ and along $u = d$. (b) Phase calculated with flat, constant-voltage electrodes (gray outlines) at $u = 0$ and von Neumann boundary conditions at $u = 0.8d$. Both produce sufficiently accurate corrector phases.

a more physical approximation to the above: we used Dirichlet boundary conditions with constant potentials along $u = 0$ only inside square, flat electrodes, and used the von Neumann boundary condition at $u = 0.8d$.

We found that, as long as the depth D was much larger than the period d, i.e. the potential is constant in z over a much longer length scale than it varies in u and v, the fringing fields were insignificant. Specifically, we found that the potential decayed exponentially with a decay length $\frac{d}{2\pi}$ outside the device. The contribution of this tail to the phase scales with d, while the contribution from inside the device scales with D. The precision of the phase can therefore be arbitrarily increased by increasing D while holding d constant, up to the limit of the thin grating condition $\lambda D \ll d^2$. As $\lambda = 1.97$ pm for 300 keV electrons, if $d = 10$ μm, the device would still act as a thin grating up to $D \sim 100$ m.

References

[1] Uchida M and Tonomura A 2010 Generation of electron beams carrying orbital angular momentum *Nature* **464** 737
[2] Verbeeck J, Tian H and Schattschneider P 2010 Production and application of electron vortex beams *Nature* **467** 301
[3] McMorran B J, Agrawal A, Anderson I M, Herzing A A, Lezec H J, McClelland J J and Unguris J 2011 Electron vortex beams with high quanta of orbital angular momentum *Science* **331** 192–5
[4] Blackburn A M and Loudon J C 2014 Vortex beam production and contrast enhancement from a magnetic spiral phase plate *Ultramicroscopy* **136** 127–43
[5] Bch A, Van Boxem R, Van Tendeloo G and Verbeeck J 2014 Magnetic monopole field exposed by electrons *Nat. Phys.* **10** 26–9
[6] Bch A, Winkler R, Plank H, Hofer F and Verbeeck J 2016 Focused electron beam induced deposition as a tool to create electron vortices *Micron* **80** 34–8
[7] Harvey T R, Pierce J S, Agrawal A K, Ercius P, Linck M and McMorran B J 2014 Efficient diffractive phase optics for electrons *New J. Phys.* **16** 093039
[8] Grillo V, Gazzadi G C, Karimi E, Mafakheri E, Boyd R W and Frabboni S 2014 Highly efficient electron vortex beams generated by nanofabricated phase holograms *Appl. Phys. Lett.* **104** 043109
[9] Shiloh R, Lereah Y, Lilach Y and Arie A 2014 Sculpturing the electron wave function using nanoscale phase masks *Ultramicroscopy* **144** 26–31
[10] Saitoh K, Hasegawa Y, Tanaka N and Uchida M 2012 Production of electron vortex beams carrying large orbital angular momentum using spiral zone plates *J. Electron Microsc.* **61** 171–7
[11] Schattschneider P, Stger-Pollach M and Verbeeck J 2012 Novel vortex generator and mode converter for electron beams *Phys. Rev. Lett.* **109** 084801
[12] Asenjo-Garcia A and Garca de Abajo F J 2014 Dichroism in the interaction between vortex electron beams, plasmons, and molecules *Phys. Rev. Lett.* **113** 066102
[13] Harvey T R, Pierce J S, Chess J J and McMorran B J 2015 Demonstration of electron helical dichroism as a local probe of chirality arXiv:1507.01810
[14] Idrobo J C and Pennycook S J 2011 Vortex beams for atomic resolution dichroism *J. Electron Microsc.* **60** 295–300
[15] Lloyd S, Babiker M and Yuan J 2012 Quantized orbital angular momentum transfer and magnetic dichroism in the interaction of electron vortices with matter *Phys. Rev. Lett.* **108** 074802
[16] Schattschneider P, Schaffer B, Ennen I and Verbeeck J 2012 Mapping spin-polarized transitions with atomic resolution *Phys. Rev.* B **85** 134422
[17] Berkhout G C G, Lavery M P J, Courtial J, Beijersbergen M W and Padgett M J 2010 Efficient sorting of orbital angular momentum states of light *Phys. Rev. Lett.* **105** 153601
[18] Lavery M P J, Robertson D J, Berkhout G C G, Love G D, Padgett M J and Courtial J 2012 Refractive elements for the measurement of the orbital angular momentum of a single photon *Opt. Express* **20** 21100

[19] Malik M, Mirhosseini M, Lavery M P J, Leach J, Padgett M J and Boyd R W 2014 Direct measurement of a 27-dimensional orbital-angular-momentum state vector *Nat. Commun.* **5** 3115
[20] Mirhosseini M, Magaa-Loaiza O S, O'Sullivan M N, Rodenburg B, Malik M, Lavery M P J, Padgett M J, Gauthier D J and Boyd R W 2015 High-dimensional quantum cryptography with twisted light *New J. Phys.* **17** 033033
[21] Yan Y *et al* 2014 High-capacity millimetre-wave communications with orbital angular momentum multiplexing *Nat. Commun.* **5** 4876
[22] Huang H *et al* 2015 Mode division multiplexing using an orbital angular momentum mode sorter and MIMO–DSP over a graded-index few-mode optical fibre *Sci. Rep.* **5** 14931
[23] Hossack W J, Darling A M and Dahdouh A 1987 Coordinate transformations with multiple computer-generated optical elements *J. Mod. Opt.* **34** 1235–50
[24] Matteucci G, Missiroli G F, Muccini M and Pozzi G 1992 Electron holography in the study of the electrostatic fields: the case of charged microtips *Ultramicroscopy* **45** 77–83
[25] Cumings J, Zettl A, McCartney M R and Spence J C H 2002 Electron holography of field-emitting carbon nanotubes *Phys. Rev. Lett.* **88** 056804
[26] Beleggia M, Kasama T, Larson D J, Kelly T F, Dunin-Borkowski R E and Pozzi G 2014 Towards quantitative off-axis electron holographic mapping of the electric field around the tip of a sharp biased metallic needle *J. Appl. Phys.* **116** 024305
[27] McCartney M R and Smith D J 2007 Electron holography: phase imaging with nanometer resolution *Ann. Rev. Mater. Res.* **37** 729–67
[28] Feynman R P 1964 The electric field in various circumstances (continued) *The Feynman Lectures on Physics* vol 2 (Reading, MA: Addison-Wesley) ch 7
[29] Pozzi G, Beleggia M, Kasama T and Dunin-Borkowski R E 2014 Interferometric methods for mapping static electric and magnetic fields *C. R. Phys.* **15** 126–39
[30] Beleggia M, Kasama T, Dunin-Borkowski R E, Hofmann S and Pozzi G 2011 Direct measurement of the charge distribution along a biased carbon nanotube bundle using electron holography *Appl. Phys. Lett.* **98** 243101
[31] Blackburn A M 2016 Observation of an electron vortex beam created from a self-charging rod *Microsc. Microanal.* **22** 1710–1